www.ietdl.org

Published in IET Generation, Transmission & Distribution
Received on 27th November 2010
Revised on 13th February 2011
doi: 10.1049/iet-gtd.2010.0779

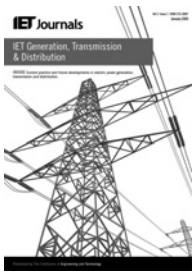

ISSN 1751-8687

Dynamic harmonic domain modelling of synchronous machine and transmission line interface

J.J. Chavez[1] *A. Ramirez*[2] *V. Dinavahi*[3]

[1]*Technical Institute of Morelia, 1550 Av. Tecnologico. Col. Lomas de Santiaguillo, Morelia, Michoacan 58120, Mexico*
[2]*Centre for Research and Advanced Studies of Mexico (CINVESTAV), 1145 Av. Del Bosque, Col. El Bajio, Zapopan, Jalisco 45019, Mexico*
[3]*University of Alberta, 9107-116 St. Edmonton, Alberta Canada, T6G 2V4*
E-mail: jchuychavez@gmail.com

Abstract: This study presents a methodology for analysing the transient behaviour of harmonics associated with the interfacing of a synchronous generator and a transmission line. The algorithm is derived entirely in the dynamic harmonic domain that is based on an orthogonal basis and on operational matrices. The main characteristics of the proposed method are: its capability to accurately follow the harmonic content of a transient without the aid of a post-processing tool and its ability to serve as a visually active indicator of the steady-state and transient conditions in a signal. The proposed method is validated by comparing its results against those obtained through a time-domain technique.

1 Introduction

The interaction between synchronous generator, transmission line and non-linear loads has a significant bearing on the power quality of a system. It is well known that the operation of a synchronous machine under non-sinusoidal conditions can produce harmonics owing to the intrinsic frequency conversion dynamics that exists between the stator and the rotor. The saturation of the rotor can enhance waveform distortion in that frequency conversion process [1–4]. In addition, the interconnection of a generator with an untransposed transmission line can produce resonances leading to over-voltages, failure of substation equipment and even power system instability [2]. Owing to the complexity of obtaining a precise model for the machine saturation [5], this subject is not considered here and left for future research work. However, accounting for enough available data, it is preliminary proposed to represent saturation as a non-linear relation, for example, a polynomial relating flux and current [6].

Several studies have been reported on the interconnection of a generator with a transmission line, a few of them dealing with harmonics [1–7]. However, most of the existing literature has focused on the steady-state analysis. The need for harmonic analysis under transient conditions arises for filtering, control and protection purposes owing to the proliferation of a variety of non-linear loads, especially fast-switching power-electronic loads.

Traditionally, electromagnetic transients' simulation tools such as EMTP and PSCAD/EMTDC can be used to calculate transients as a function of time. A post-processing routine can then be used to compute the corresponding harmonic content during the period of interest. For the sake of an example, the windowed fast Fourier transform (WFFT) allows the calculation of the harmonic content of a signal as a function of time by sliding an FFT window. However, numerical errors such as aliasing, Gibbs oscillations and the picket-fence effect [8] make such techniques unattractive for relatively fast transients.

A harmonic domain (HD) methodology, based on constant Fourier coefficients, was pioneered by Xia and Heydt, using a decoupled positive sequence circuit for a full-wave bridge rectifier [9, 10]. Later on, Densem *et al.* reported that the network must be modelled in the *abc* frame since the characteristic harmonics cannot be properly evaluated by a positive sequence frequency representation [11]. The HD methodology was extended to the dynamic case, that is, with variable Fourier coefficients, for transient studies by Acha *et al.* [6], and it is hereafter referred to as the dynamic harmonic domain (DHD) methodology.

The DHD is a direct approach for transient and steady-state solution of harmonics. It is based on an orthogonal basis and on operational matrices, with the coefficients of the orthogonal basis being the state variables. Intrinsically, the DHD solution allows the possibility of computing the evolution of the harmonic coefficients step-by-step. In addition, the DHD methodology provides the power quality indices used in steady-state applications as functions of time.

In this paper, we propose a methodology for directly analysing the transient behaviour of harmonics in a generator-line load system using the DHD without resorting to post-processing techniques for harmonic tracking. In the generator model, both the electromechanical and the electromagnetic dynamics are taken into account and are coupled numerically through a hybrid numerical solution. For illustration purposes a single-mass model is considered;

however, the extension to the multi-mass case is straightforward. The untransposed transmission line is modelled as a fully frequency-dependent line. In this work we have taken the DHD line model proposed in [12]. Linear and non-linear loads are interfaced to the system via their corresponding differential/algebraic equations. The simulation results from the proposed method are validated through a time-domain technique. The former can potentially be implemented in real-time simulation by using efficient technologies such as field programmable gate arrays (FPGAs) and graphic processor units (GPUs), thus overcoming the network's size restriction.

The paper is organised as follows. In Section 2, the DHD models for synchronous machine, the transmission line and their interconnection are presented. The algorithm proposed for the numerical solution of the complete system is explained in Section 3. Section 4 analyses the simulation results for an example system under various transient conditions. Section 5 presents the conclusions of the study.

2 Generator and transmission line DHD models

This section outlines the modelling of the synchronous generator and the transmission line in the DHD and describes the interfacing of the two models.

2.1 Generator

The following definition is used

$$\theta = \omega_o t + \theta_{\text{rel}} \tag{1}$$

where ω_o is the electrical power angular frequency in rad/s and θ_{rel} corresponds to the deviation (from its uniformly rotating reference on phase a) of the rotor angle θ (defined as the angle between phase a and the d-axis).

The synchronous machine can be represented in the time domain (using motor convention) as

$$\begin{bmatrix} \boldsymbol{v}_{\text{s}} \\ \boldsymbol{v}_{\text{r}} \end{bmatrix} = \begin{bmatrix} \boldsymbol{R}_{\text{s}} & \\ & \boldsymbol{R}_{\text{r}} \end{bmatrix} \begin{bmatrix} \boldsymbol{i}_{\text{s}} \\ \boldsymbol{i}_{\text{r}} \end{bmatrix} + \frac{d}{dt} \begin{bmatrix} \Psi_{\text{s}} \\ \Psi_{\text{r}} \end{bmatrix} \tag{2}$$

where the s and r subscripts correspond to stator and rotor quantities, respectively. In the DHD (2) becomes (without change of notation)

$$\begin{bmatrix} \boldsymbol{v}_{\text{s}} \\ \boldsymbol{v}_{\text{r}} \end{bmatrix} = \boldsymbol{L} \frac{\text{d}}{\text{d}t} \begin{bmatrix} \boldsymbol{i}_{\text{s}} \\ \boldsymbol{i}_{\text{r}} \end{bmatrix} + \left(\boldsymbol{R} + \boldsymbol{L}\boldsymbol{S}_{\text{sr}} + \frac{\text{d}}{\text{d}\theta}\boldsymbol{L} \right) \begin{bmatrix} \boldsymbol{i}_{\text{s}} \\ \boldsymbol{i}_{\text{r}} \end{bmatrix} \tag{3}$$

where (using Matlab® notation)

$$\boldsymbol{L} = \begin{bmatrix} \boldsymbol{L}_{\text{s}} & \boldsymbol{L}_{\text{sr}} \\ \boldsymbol{L}_{\text{rs}} & \boldsymbol{L}_{\text{r}} \end{bmatrix}, \quad \boldsymbol{R} = \text{blkdiag}\{\boldsymbol{R}_{\text{s}}, \boldsymbol{R}_{\text{r}}\}$$

$$\boldsymbol{S}_{\text{sr}} = \text{blkdiag}\{\boldsymbol{S}_{\text{s}}, \boldsymbol{S}_{\text{r}}\}$$

$$\boldsymbol{S}_{\text{s}} = \text{blkdiag}\{\boldsymbol{S}, \boldsymbol{S}, \boldsymbol{S}\}, \quad \boldsymbol{S}_{\text{r}} = \{\boldsymbol{S}'_{\text{r}}, \boldsymbol{S}'_{\text{r}}, \boldsymbol{S}'_{\text{r}}, \boldsymbol{S}'_{\text{r}}\}$$

$$\boldsymbol{S} = \text{diag}\{\ldots, -3j\omega_o, -j\omega_o, j\omega_o, 3j\omega_o, \ldots\}$$

$$\boldsymbol{S}'_{\text{r}} = \text{diag}\{\ldots, -4j\omega_o, -2j\omega_o, 0, 2j\omega_o, 4j\omega_o, \ldots\}$$

In (3), the vectors representing stator and rotor voltages and currents are time-varying harmonic vectors, whereas the inductance and resistance matrices are Toeplitz-type matrices [6]. The steady-state solution can be obtained by setting to zero the derivatives with respect to time in (3).

Alternatively, (3) can be expressed in a compact form as

$$\frac{\text{d}}{\text{d}t} \begin{bmatrix} \boldsymbol{i}_{\text{s}} \\ \boldsymbol{i}_{\text{r}} \end{bmatrix} = \boldsymbol{A}_{\text{g}} \begin{bmatrix} \boldsymbol{i}_{\text{s}} \\ \boldsymbol{i}_{\text{r}} \end{bmatrix} + \boldsymbol{L}^{-1} \begin{bmatrix} \boldsymbol{v}_{\text{s}} \\ \boldsymbol{v}_{\text{r}} \end{bmatrix} \tag{4}$$

where

$$\boldsymbol{A}_{\text{g}} = -\boldsymbol{L}^{-1} \left(\boldsymbol{R} + \boldsymbol{L}\boldsymbol{S}_{\text{sr}} + \frac{\text{d}}{\text{d}\theta}\boldsymbol{L} \right)$$

The mechanical dynamics of the machine is described (for a single-mass rotor) as follows

$$\dot{\omega}_{\text{rel}} = \frac{\omega_o}{2H} [T_{\text{e}} - T_m + k_d \omega_{\text{rel}}] \tag{5a}$$

$$\dot{\theta} = \omega_{\text{rel}} \tag{5b}$$

where

$$T_{\text{e}} = \frac{1}{2} \boldsymbol{i}^{\text{T}} \frac{\text{d}\boldsymbol{L}}{\text{d}\theta} \boldsymbol{i} \tag{6}$$

In (6), the current vector, $\boldsymbol{i}$, contains both stator and rotor currents. From (6) one can notice that the complete set of harmonics contribute to the scalar electrical torque T_{e}.

2.2 Transmission line

Since the underlying idea of this work is to analyse transients accurately, the DHD transmission line model used here is based on a frequency-dependent line model in the phase domain [13], where the propagation matrix and the characteristic admittance are approximated by rational functions using vector fitting [14] (see Appendix 1). The corresponding propagation equations in the time domain are (see Fig. 1*a* for reference directions) [12]

$$\begin{bmatrix} \dot{\boldsymbol{x}}_1 \\ \dot{\boldsymbol{x}}_2 \end{bmatrix} = \begin{bmatrix} \boldsymbol{A}_1 & \\ & \boldsymbol{A}_1 \end{bmatrix} \begin{bmatrix} \boldsymbol{x}_1 \\ \boldsymbol{x}_2 \end{bmatrix} + \begin{bmatrix} \boldsymbol{b}_1 & \\ & \boldsymbol{b}_1 \end{bmatrix} \begin{bmatrix} \boldsymbol{i}'_n \\ \boldsymbol{i}'_m \end{bmatrix} \tag{7a}$$

$$\begin{bmatrix} \boldsymbol{i}'_n \\ \boldsymbol{i}'_m \end{bmatrix} = \begin{bmatrix} \boldsymbol{c}_1 & \\ & \boldsymbol{c}_1 \end{bmatrix} \begin{bmatrix} \boldsymbol{x}_1 \\ \boldsymbol{x}_2 \end{bmatrix} \tag{7b}$$

with their counterpart in the DHD given by [12]

$$\begin{bmatrix} \dot{\boldsymbol{x}}_1 \\ \dot{\boldsymbol{x}}_2 \end{bmatrix} = \begin{bmatrix} \boldsymbol{A}_1 - \boldsymbol{S}' & \\ & \boldsymbol{A}_1 - \boldsymbol{S}' \end{bmatrix} \begin{bmatrix} \boldsymbol{x}_1 \\ \boldsymbol{x}_2 \end{bmatrix} + \begin{bmatrix} \boldsymbol{B}_1\Gamma & \\ & \boldsymbol{B}_1\Gamma \end{bmatrix} \begin{bmatrix} \boldsymbol{i}'_n \\ \boldsymbol{i}'_m \end{bmatrix} \tag{8a}$$

$$\begin{bmatrix} \boldsymbol{i}'_n \\ \boldsymbol{i}'_m \end{bmatrix} = \begin{bmatrix} \boldsymbol{C}_1 & \\ & \boldsymbol{C}_1 \end{bmatrix} \begin{bmatrix} \boldsymbol{x}_1 \\ \boldsymbol{x}_2 \end{bmatrix} \tag{8b}$$

It is mentioned here that after calculating $\boldsymbol{i}'_m$ and $\boldsymbol{i}'_n$ and in the modal domain, they are transformed into the phase domain.

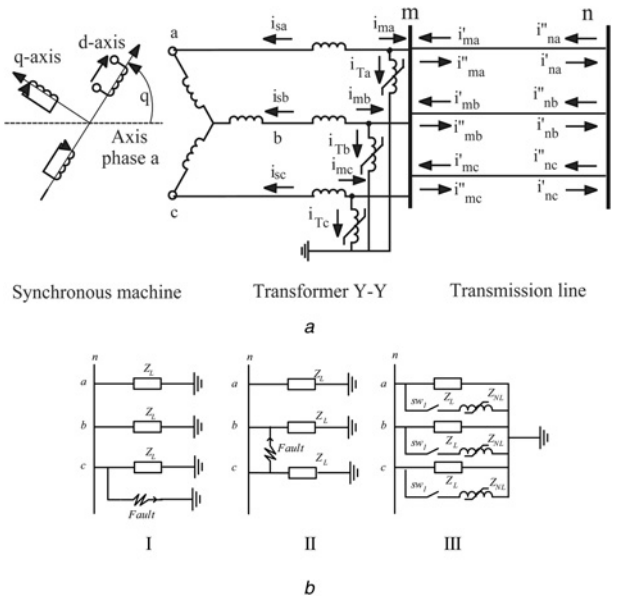

Fig. 1 *Test case*

a Network system
b Single-phase-to-ground fault (I), line-to-line fault (II) and three-phase non-linear load (III)

In addition to the propagation equations, we have the terminal equations for bus m [12]

$$\dot{\boldsymbol{x}}_3 = (\boldsymbol{A}_2 - \boldsymbol{S})\boldsymbol{x}_3 + \boldsymbol{B}_2\boldsymbol{v}_m \tag{9a}$$

$$\boldsymbol{i}_m = \boldsymbol{C}_2\boldsymbol{x}_3 + \boldsymbol{D}_2\boldsymbol{v}_m - 2\boldsymbol{i}'_m \tag{9b}$$

Similarly, for bus n we have

$$\dot{\boldsymbol{x}}_4 = (\boldsymbol{A}_2 - \boldsymbol{S})\boldsymbol{x}_4 + \boldsymbol{B}_2\boldsymbol{v}_n \tag{10a}$$

$$\boldsymbol{i}_n = \boldsymbol{C}_2\boldsymbol{x}_4 + \boldsymbol{D}_2\boldsymbol{v}_n - 2\boldsymbol{i}'_n \tag{10b}$$

The reflected currents are updated at each time step with

$$\boldsymbol{i}''_m = \boldsymbol{i}'_m + \boldsymbol{i}_m \tag{11a}$$

$$\boldsymbol{i}''_n = \boldsymbol{i}'_n + \boldsymbol{i}_n \tag{11b}$$

2.3 Interfacing

The resulting DHD ordinary differential equations for the line are now interfaced to a transformer (its magnetising branch taken here as a non-linear inductance [15]) and the machine equations.

From the output expression of (9b) the relation between sending end voltage and current is given by (note that $m = -(\boldsymbol{i}_s + \boldsymbol{i}_T)$ and $\boldsymbol{v}_s = \boldsymbol{v}_m$)

$$\boldsymbol{v}_s = \boldsymbol{D}_2^{-1}(2\boldsymbol{i}'_s - \boldsymbol{C}_2\boldsymbol{x}_3 - \boldsymbol{i}_s - \boldsymbol{i}_T) \tag{12}$$

Substituting (12) into (9a), the transmission line, the transformer and the generator models are linked as

$$\dot{\boldsymbol{x}}_3 = (\boldsymbol{A}_2 - \boldsymbol{S} - \boldsymbol{B}_2\boldsymbol{D}_2^{-1}\boldsymbol{C}_2)\boldsymbol{x}_3 + 2\boldsymbol{B}_2\boldsymbol{D}_2^{-1}\boldsymbol{i}'_s - \boldsymbol{B}_2\boldsymbol{D}_2^{-1}(\boldsymbol{i}_s + \boldsymbol{i}_T) \tag{13}$$

taking into account (4) and (13) gives

$$\frac{\mathrm{d}}{\mathrm{d}t}\begin{bmatrix}\boldsymbol{i}_s\\ \boldsymbol{i}_r\end{bmatrix} = \boldsymbol{G}_m\begin{bmatrix}\boldsymbol{i}_s\\ \boldsymbol{i}_r\end{bmatrix} + \boldsymbol{L}_{g1}^{-1}\boldsymbol{D}_2^{-1}[-\boldsymbol{C}_2\boldsymbol{x}_3 + 2\boldsymbol{C}_2\boldsymbol{i}'_s - (\alpha_T\Phi_T + \beta_T\Phi_T^3)] + \boldsymbol{L}_{g1}^{-1}\boldsymbol{v}_r \tag{14}$$

where

$$\boldsymbol{G}_m = -\boldsymbol{L}_{g1}^{-1}\left\{\begin{bmatrix}\boldsymbol{R}_s + \boldsymbol{D}_2^{-1} & \\ & \boldsymbol{R}_r\end{bmatrix} + \boldsymbol{L}\boldsymbol{S}_{sr} + \frac{\mathrm{d}}{\mathrm{d}\theta}\boldsymbol{L}\right\}$$

It is mentioned that the magnetising branch of the transformer has been represented as the flux/current relation: $\boldsymbol{i}_T = (\alpha_T\Phi_T + \beta_T\Phi_T^3)$. Combining (13) and (14) into a state–space representation, we finally obtain (15)

$$\begin{bmatrix} -\boldsymbol{G}_m & -\boldsymbol{L}_{g1}^{-1}\boldsymbol{D}_2^{-1}\boldsymbol{C}_2 & \boldsymbol{L}_{g1}^{-1}\boldsymbol{D}_2^{-1}(\alpha_T + \beta_T\Phi_T)\\ \begin{bmatrix}\boldsymbol{B}_2\boldsymbol{D}_2^{-1} & 0\end{bmatrix} & \boldsymbol{A}_2 - \boldsymbol{S} - \boldsymbol{B}_2\boldsymbol{D}_2^{-1}\boldsymbol{C}_2 & \boldsymbol{B}_2\boldsymbol{D}_2^{-1}(\alpha_T + \beta_T\Phi_T)\\ \begin{bmatrix}-\boldsymbol{D}_2^{-1} & 0\end{bmatrix} & -\boldsymbol{D}_2^{-1}\boldsymbol{C}_2 & \boldsymbol{D}_2^{-1}(\alpha_T + \beta_T\Phi_T)\end{bmatrix} \times \begin{bmatrix}\boldsymbol{i}_s\\ \boldsymbol{i}_r\\ \boldsymbol{x}_3\\ \Phi_T\end{bmatrix} + \begin{bmatrix}2\boldsymbol{L}_{g1}^{-1}\boldsymbol{D}_2^{-1} & \boldsymbol{L}_{g2}^{-1}\\ 2\boldsymbol{B}_2\boldsymbol{D}_2^{-1} & 0\\ 2\boldsymbol{D}_2^{-1} & 0\end{bmatrix}\begin{bmatrix}\boldsymbol{i}'_s\\ \boldsymbol{v}_r\end{bmatrix} = \frac{\mathrm{d}}{\mathrm{d}t}\begin{bmatrix}\boldsymbol{i}_s\\ \boldsymbol{i}_r\\ \boldsymbol{x}_3\\ \Phi_T\end{bmatrix} \tag{15}$$

3 DHD algorithm for transient harmonic analysis

The complete set of ODEs representing the generator-transformer-line system given by (5), (8a) and (15) can be expressed in compact form as

$$\begin{bmatrix}\dot{\boldsymbol{x}}_e\\ \dot{\boldsymbol{x}}_m\end{bmatrix} = \begin{bmatrix}\boldsymbol{A}_e & \\ & \boldsymbol{A}_m\end{bmatrix}\begin{bmatrix}\boldsymbol{x}_e\\ \boldsymbol{x}_m\end{bmatrix} + \begin{bmatrix}\boldsymbol{B}_e\\ \boldsymbol{B}_m\end{bmatrix}\boldsymbol{u} \tag{16}$$

where $\boldsymbol{x}_e$ and $\boldsymbol{x}_m$ represent the harmonic vectors of electrical and mechanical state variables, respectively. Since the generator contains slow and fast dynamics at the same time, a hybrid algorithm is used for the numerical integration of (16) such that the stiffness of the complete system is overcome. The algorithm consists of the following four steps:

Step 1: Assume that the simulation begins with the system in steady state. Initialise all the system variables.
Step 2: Using the trapezoidal rule for (16) the electrical state variables and the electrical torque are calculated at Steps $k+1$ and $k+1/2$ by

$$\boldsymbol{m}_1\boldsymbol{x}_e^{k+1} = \boldsymbol{m}_2\boldsymbol{x}_e^k + \frac{\boldsymbol{B}_e^k}{2}(\boldsymbol{u}_k + \boldsymbol{u}_{k+1}) \tag{17a}$$

$$\boldsymbol{n}_1\boldsymbol{x}_e^{k+1/2} = \boldsymbol{n}_2\boldsymbol{x}_e^k + \frac{\boldsymbol{B}_e^k}{2}(\boldsymbol{u}_k + \boldsymbol{u}_{k+1/2}) \tag{17b}$$

where

$$\boldsymbol{m}_{1,2} = \left(\frac{1}{\Delta t}\boldsymbol{I} \mp \frac{1}{2}\boldsymbol{A}_e^k\right), \quad \boldsymbol{n}_{1,2} = \left(\frac{2}{\Delta t}\boldsymbol{I} \mp \frac{1}{2}\boldsymbol{A}_e^k\right)$$

doi: 10.1049/iet-gtd.2010.0779

and

$$\boldsymbol{x}_{\mathrm{e}}^{k} = [\boldsymbol{x}_1, \boldsymbol{x}_2, \boldsymbol{x}_3, \Phi_T, \boldsymbol{i}_{\mathrm{r}}, \boldsymbol{i}_{\mathrm{s}}]^{\mathrm{T}}$$

The electrical torque is obtained by

$$T_{\mathrm{e}}^{k+1/2} = \frac{1}{2}\boldsymbol{i}_{\mathrm{s},k+1/2}^{\mathrm{T}} \frac{\mathrm{d}}{\mathrm{d}\theta}\boldsymbol{L}^{k+1/2}\boldsymbol{i}_{\mathrm{s},k+1/2} \tag{18}$$

Step 3: First, a predicted value of ω_{rel} is given by

$$p_1\hat{\omega}_{\mathrm{rel}}^{k+3/2} = p_2\omega_{\mathrm{rel}}^{k+1/2} + \frac{\omega_o}{2H}(T_{\mathrm{e}}^{k+1/2} - T_m) \tag{19}$$

where $p_{1,2} = (1/\Delta t) \mp \omega_o k_d/4H$.

Then, a corrected value for θ_{rel} is obtained by

$$\theta_{\mathrm{rel}}^{k+3/2} = \theta_{\mathrm{rel}}^{k+1/2} + \frac{\Delta t}{2}(\hat{\omega}_{\mathrm{rel}}^{k+3/2} + \omega_{\mathrm{rel}}^{k+1/2}) - \omega_o\Delta t \tag{20}$$

Finally, with $\hat{\omega}_{\mathrm{rel}}^{k+3/2}$ and $\theta_{\mathrm{rel}}^{k+3/2}$ calculate the inductance matrix $(\mathrm{d}/\mathrm{d}\theta)\boldsymbol{L}_{\theta}^{k+3/2}$ with

$$\frac{\mathrm{d}}{\mathrm{d}\theta}\boldsymbol{L}_{\theta}^{k+1} = \left(\frac{\mathrm{d}}{\mathrm{d}\theta}\boldsymbol{L}_{\theta}^{k+1/2} + \frac{\mathrm{d}}{\mathrm{d}\theta}\boldsymbol{L}_{\theta}^{k+3/2}\right)/2 \tag{21}$$

Step 4: The average values of the electrical states and torque are computed as

$$\boldsymbol{x}_{\mathrm{e}\,a} = (\boldsymbol{x}_{\mathrm{e}}^{k+1/2} + \boldsymbol{x}_{\mathrm{e}}^{k+1})/2 \tag{22a}$$

$$T_{\mathrm{e}\,a} = \frac{1}{2}\boldsymbol{x}_{\mathrm{e}\,a}^{T}\frac{\mathrm{d}}{\mathrm{d}\theta}\boldsymbol{L}^{k+1}\boldsymbol{x}_{\mathrm{e}\,a} \tag{22b}$$

$$p_1\omega_{\mathrm{rel}}^{k+3/2} = p_1\omega_{\mathrm{rel}}^{k+1/2} + \frac{\omega_o}{2H}(T_{\mathrm{e}\,a} - T_m) \tag{22c}$$

4 Case study

To ascertain the accuracy of the proposed algorithm, a case study is presented. The results provided here were compared against those obtained by a time-domain technique, which consists in solving the original non-linear ODEs by numerical integration (labelled as TD in the corresponding figures).

Fig. 1 shows the test case where a 555 MVA, 24 kV synchronous machine is connected to a solidly grounded $Y-Y$ transformer with $L_T = 0.02$ pu, $\alpha_T = 0.02$ pu and $\beta_T = 8 \times 10^4$ pu to a 100 km open-ended transmission line. The geometry of the untransposed line is shown in Appendix 2. The synchronous machine parameters were obtained from [5] where the per unit parameters have been calculated on the basis of the machine nominal power and voltage (i.e. 555 MVA and 24 kV). Simulation results for steady-state as well as transient conditions are analysed in the following subsections.

4.1 Steady state

Fig. 2 (reproduced using the method in [2]) corresponds to the steady-state voltage for a generator and an open-ended line system showing the magnitude of its harmonics when the length of the line is varied from 10 to 1000 km. From Fig. 2 one can notice several harmonic resonance conditions, the most noticeable around 147.8 km line

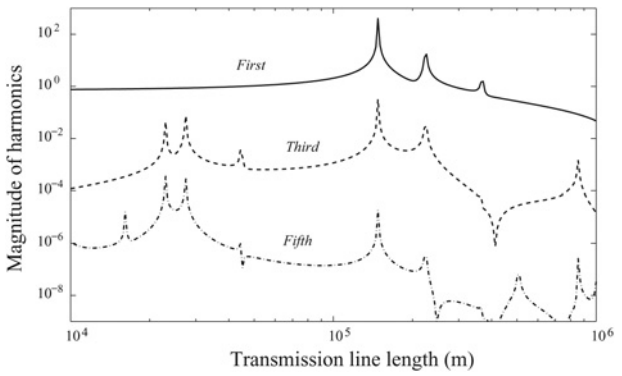

Fig. 2 *Harmonic behaviour of the steady-state voltage v_{ma} for the open-ended line with varying line lengths*

length. The results in Fig. 2 have been further corroborated for several line lengths with the proposed DHD model described in Section 2 by setting to zero all the derivatives with respect to time. This HD computation permits to calculate initial conditions that can be included in the DHD.

4.2 Single-phase fault

The simulation starts in steady state with the far end of the line having a load with $R = 125$ pu, $L = 1$ pu. After 0.0332 s, phase c is connected to ground through a 10^{-8} pu resistance to simulate a phase-to-ground fault. Then, at 0.085 s the fault is cleared and the same RL load is reconnected until a new steady state is reached (see Fig. 1*b*-I). The instantaneous voltage waveforms at the receiving line terminal, phase c, v_{nc}, from both the DHD and the TD, are presented in Fig. 3. The stator currents $\boldsymbol{i}_{\mathrm{s}}$ are shown in Fig. 4*a*. In addition, the corresponding harmonic content for phase c obtained through the DHD is presented in Fig. 4*b*. For the DHD simulation up to the ninth harmonic was considered since the magnitudes of the remaining harmonics were negligible. It is mentioned that in this paper the figures corresponding to harmonic content present only the harmonics with considerable magnitude with respect to the fundamental frequency.

Although some harmonics behave as very small quantities in a specific condition, in resonance conditions

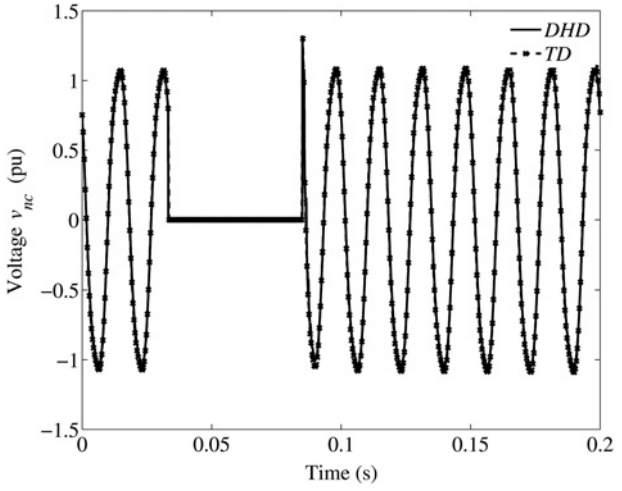

Fig. 3 *Voltage v_{nc} during the single-phase fault*

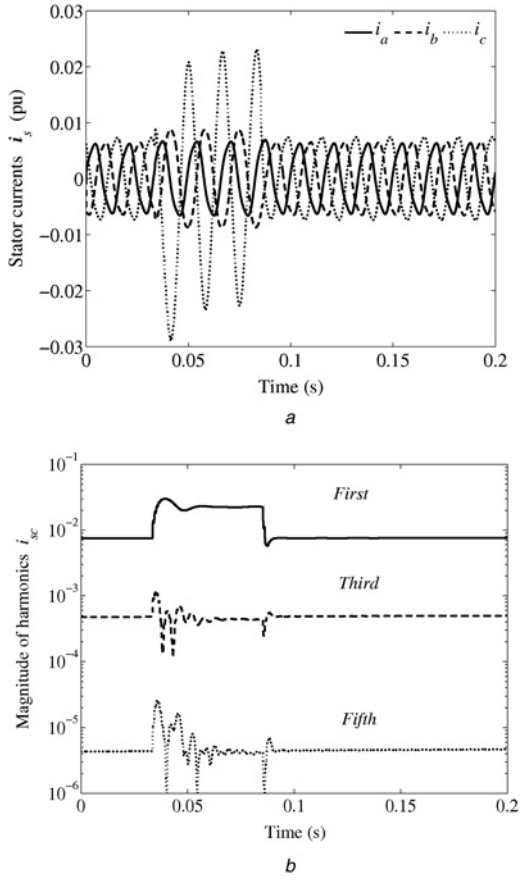

Fig. 4 *Stator currents during the single-phase fault*

a Stator currents i_s
b Harmonic content of i_{sc}

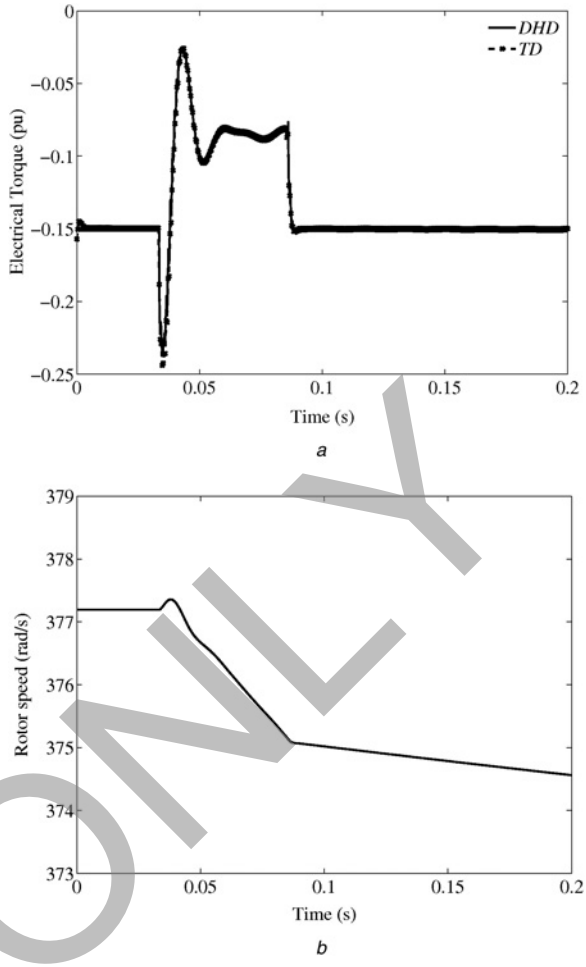

Fig. 5 *Mechanical parameters during the single-phase fault*

a Machine electrical torque
b Rotor speed

their magnitudes can be increased considerably (see Fig. 2). Furthermore, when electronic devices are connected to the network, some of the devices' characteristic harmonics (different than the fundamental) will be an important part of the solution. The proposed methodology has the flexibility of including any number of harmonics.

Additionally, the electrical torque from both DHD and TD are presented in Fig. 5*a*, and the machine speed obtained by the DHD technique is shown in Fig. 5*b*.

4.3 Phase-to-phase fault

A phase-to-phase fault is simulated between phases *b* and *c* as illustrated in Fig. 1*b*-II. The simulation starts in steady state and after the second cycle a fault is inserted through a 10^{-8} pu resistance. Finally, after another three cycles the fault is cleared. Fig. 6*a* shows the current at bus *n*, phase *b* (i_{nb}), and Fig. 7*a* presents the voltages at the end of the line for all phases (v_{na}, v_{nb} and v_{nc}) with the harmonic content of phase *b* shown in Figs. 6*b* and 7*b*. From Figs. 6 and 7 one can notice that the system tries to reach a different steady state sequentially.

4.4 Three-phase non-linear load

The proposed methodology is now applied to the network in Fig. 1*a* with a non-linear reactor as a load. The time-domain representation of the chosen non-linear load is given by the flux/current relation $i(t) = f(\varphi)$ and expressed, without losing generality, as a polynomial (in the DHD) of the type

$$\boldsymbol{i} = \alpha\Phi + \beta\Phi^{p} \tag{23}$$

The power p is related to a convolution operation in (23) [6, 12]. As mentioned earlier, a similar representation has been taken here for the magnetising branch of the transformer [15].

The current expression for a resistive load in parallel with a non-linear reactor at bus *n*, as shown in Fig. 1*b*-III, is given by

$$\boldsymbol{i}_n = -\alpha\Phi - \beta\Phi^{p} - \boldsymbol{R}^{-1}\boldsymbol{v}_n \tag{24}$$

Substituting (24) into (10b) gives

$$\boldsymbol{v}_n = K(-\alpha\Phi - \beta\Phi^{p} - \boldsymbol{C}_2\boldsymbol{x}_4 + 2\boldsymbol{i}'_n) \tag{25}$$

where $\boldsymbol{K} = (\boldsymbol{I} + \boldsymbol{R}\boldsymbol{D}_2)^{-1}\boldsymbol{R}$ and $\boldsymbol{R}$ is the linear load. Next, substituting (25) into (10a) and taking the following DHD voltage/flux relation into account

$$\dot{\Phi} - \boldsymbol{S}\Phi = \boldsymbol{v}_n \tag{26}$$

doi: 10.1049/iet-gtd.2010.0779

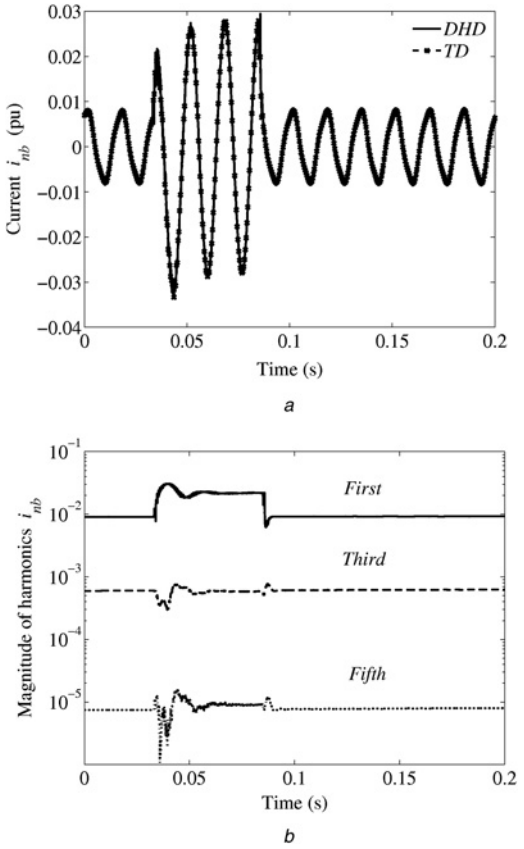

Fig. 6 *Current at bus n phase b during the phase-to-phase fault*
a Current i_{nb}
b Harmonic content of i_{nb}

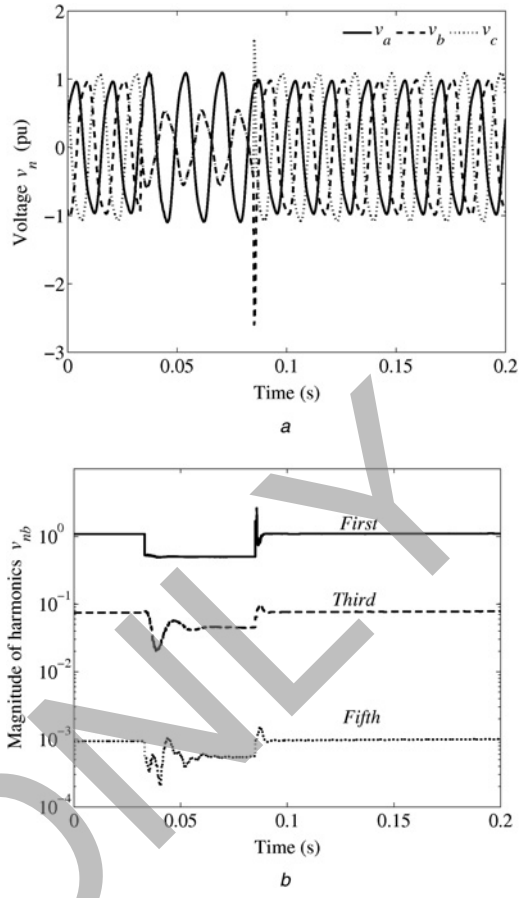

Fig. 7 *Voltages at bus n during the phase-to-phase fault*
a Voltages v_n
b Harmonic content of v_{nb}

We obtain the final current/flux relation for bus $\boldsymbol{n}$ as

$$\begin{bmatrix} \boldsymbol{A}_2 - \boldsymbol{S}' - K\boldsymbol{B}_2\boldsymbol{C}_2 & -K\boldsymbol{B}_2(\alpha + \beta\Phi^{p-1}) \\ -K\boldsymbol{C}_2 & -\boldsymbol{S} - K(\alpha + \beta\Phi^{p-1}) \end{bmatrix} \times \begin{bmatrix} \boldsymbol{x}_4 \\ \Phi \end{bmatrix} + 2K \begin{bmatrix} \boldsymbol{B}_2 \\ \boldsymbol{I}_h \end{bmatrix} \boldsymbol{i}'_n = \begin{bmatrix} \dot{\boldsymbol{x}}_4 \\ \dot{\Phi} \end{bmatrix} \quad (27)$$

Finally, (27) is introduced into (16) as part of the harmonic vector of electrical state variables $\boldsymbol{x}_e$.

For this example the simulation starts in steady state and after 0.0332 s, a non-linear load ($\alpha = 0.5$, $\beta = 8 \times 10^6$) in parallel to the 125 pu resistance is connected in each phase at bus n. The simulation ends at 0.15 s. In Fig. 8, the voltage at bus n phase a and the corresponding harmonic content are shown. As expected, one can notice from these figures that the harmonic distortion is larger when non-linear loads are introduced into the network. In fact, the waveform in Fig. 8*a* presents 16.9 and 2.5% of the third and fifth harmonic, respectively.

4.5 Accuracy of the proposed technique

Accuracy of the DHD depends on both, size of the time step and the number of harmonics. To the best of the authors' knowledge, in the literature regarding harmonics, there is not a criterion for determining the number of harmonics given a predefined error and is still a research-open topic. Nevertheless, the knowledge of the harmonic content of the source (or perturbation) and/or the amount of non-linearity involved, given, for instance, by the α and β coefficients in the polynomial type flux/current relation can shade light on such number. Additionally, the highest harmonic is closely related to the time step used for the simulation. A steady state solution using the HD can be used to figure out the approximate number of harmonic coefficients required in a dynamic study.

Fig. 9*a* shows the rotor currents $\boldsymbol{i}_r$ and its various components: i_F is the field winding current, which produces flux in the direct axis (connected to the DC source of the excitation system); i_D is the quadrature axis winding current to represent slowly changing fluxes produced by deep-flowing eddy currents; i_G and i_Q are the direct and quadrature axes winding currents to represent damping bar effects.

Fig. 9*b* shows the harmonic content of i_G, where only even harmonics appear owing to the DC source excitation. Some remarks regarding the obtained results:

1. During steady state all harmonics behave as constants, as expected.
2. Harmonics react instantaneously to system disturbances. Their dynamics are followed in a natural way by the DHD while post-processing techniques (for instance, WFFT) would have a slow harmonic tracking response.
3. The proportionality of harmonic magnitudes for a given signal (voltage or current) changes from steady state to the transient state.

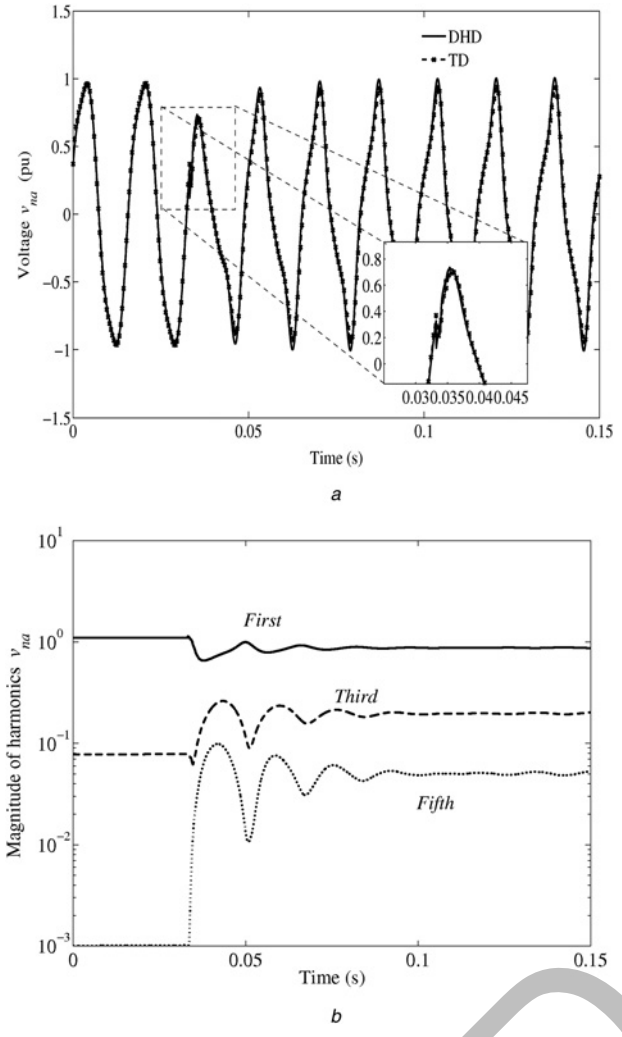

Fig. 8 *Voltage at bus n phase a for a three-phase non-linear load*
a Voltage v_{na}
b Harmonic content of v_{na}

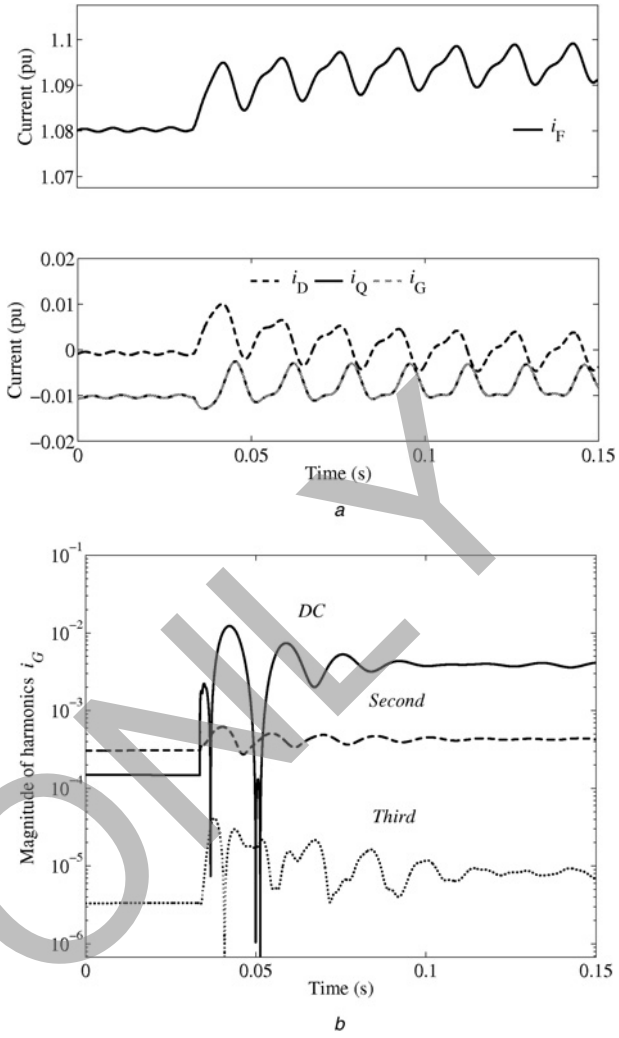

Fig. 9 *Rotor currents for a three-phase non-linear load*
a Rotor currents i_r
b Harmonic content of i_G

4. Harmonic oscillations during a transient behave according to the line resonant frequency, travelling time and excitation-related frequencies.
5. After removing a fault, steady state is reached faster by lower harmonics than by higher harmonics.
6. Simply examining the time-domain results, it is difficult to discern the steady-state condition. The DHD provides a visually active indicator of the transient and steady-state conditions in a signal.

4.6 Power quality indices

Power quality assessment under transient conditions has a significant impact for the design of active filters. However, the traditional method of using windowed FFT does not yield accurate harmonic information under transient conditions. The DHD allows obtaining the power quality indices directly through traditional formulae [6].

As an example, Fig. 10 shows the evolution of the most used power quality indices (power factor and distortion factors can also be derived) for the 100 km line example with a non-linear load. As expected, the quantities are constants in periodic steady state and register significant changes during transient conditions owing to the dynamic harmonics behaviour. Further potential applications of the proposed model to the power quality area can be seen in [16].

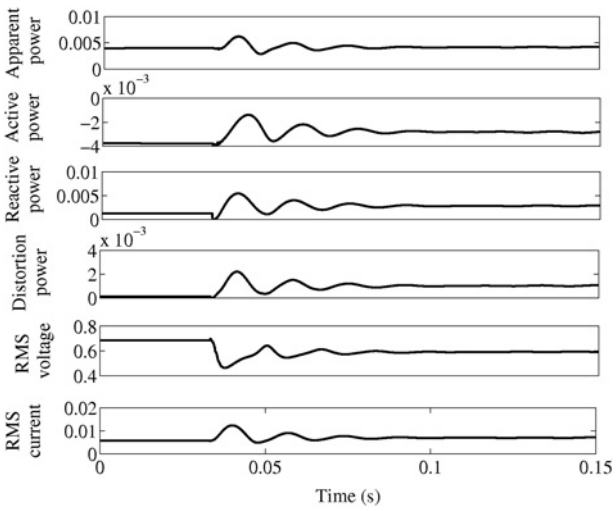

Fig. 10 *Power quality parameters for bus n with a three phase non-linear load*

doi: 10.1049/iet-gtd.2010.0779

5 Conclusions

This paper has presented the interfacing of the synchronous generator and an untransposed transmission line for analysing harmonics behaviour under transient conditions. The proposed algorithm is based on the dynamic harmonic domain (DHD) methodology, which permits following step-by-step the harmonics evolution with respect to time. Additionally, it has been corroborated that the time-varying harmonic coefficients are capable of representing the non-harmonic line frequencies involved in the transient [12]. The proposed algorithm can handle non-linear loads in a straightforward manner while in frequency-domain techniques the inclusion of such loads is still difficult. The accuracy of the proposed algorithm was verified for a single machine-line load system; however, the method is applicable to longer systems as well, provided enough computational resources are available. This is because in the DHD, the size of the ODEs system becomes large as the instantaneous variables are transformed into harmonic vectors. Nevertheless, the algorithm can be potentially used in real-time simulation. The applications of the algorithm include the study of harmonics in transient state for control, protection and power quality purposes and also in the study of ferroresonance.

6 Acknowledgment

This work was supported in part by the National Council of Science and Technology (CONACYT-FOMIXJAL-51689) Mexico.

7 References

1 Semlyen, A., Eggleston, J.F., Arrillaga, J.: 'Admittance matrix model of a synchronous machine for harmonic analysis', *IEEE Trans. Power Syst.*, 1987, **PAS-2**, (4), pp. 833–840
2 Ramirez, A., Semlyen, A., Iravani, R.: 'Harmonic domain characterization of the resonant interaction between generator and transmission line', *IEEE Trans. Power Deliv.*, 2005, **20**, (3), pp. 1753–1762
3 Semlyen, A., Acha, E., Arrillaga, J.: 'Newton type algorithms for the harmonic phasor analysis of nonlinear power circuits in periodical steady state with special reference to magnetic nonlinearities', *IEEE Trans. Power Deliv.*, 1988, **3**, (3), pp. 1090–1098
4 Chen, H., Long, Y., Zhang, X.P.: 'More sophisticated synchronous machine model and the relevant harmonic power flow study', *IEE Proc. Gener. Transm. Distrib.*, 1999, **146**, (3), pp. 261–268
5 Kundur, P.: 'Power system stability and control' (McGraw-Hill, USA, 1993)
6 Rico, J.J., Madrigal, M., Acha, E.: 'Dynamic harmonic evolution using the extended harmonic domain', *IEEE Trans. Power Deliv.*, 2003, **18**, (2), pp. 587–594
7 Stankovic, A.M., Sanders, S.R., Aydin, T.: 'Dynamic phasors in modeling and analysis of unbalanced polyphase AC machines', *IEEE Trans. Energy Convers.*, 2002, **18**, (1), pp. 107–113
8 Proakis, J.G., Manolakis, D.G.: 'Digital signal processing: principles, algorithms, and applications' (Prentice Hall, NJ, 1996)
9 Xia, D., Heydt, G.T.: 'Harmonic power flow studies – part I: formulation and solution', *IEEE Trans. Power Appl. Syst.*, 1982, **PAS-101**, pp. 1257–1265
10 Xia, D., Heydt, G.T.: 'Harmonic power flow studies – part II: implementation and practical application', *IEEE Trans. Power Appl. Syst.*, 1982, **PAS-101**, pp. 1266–1270
11 Densem, T.J., Bodger, P.S., Arrillaga, J.: 'Three phase transmission system modeling for harmonic penetration studies', *IEEE Trans. Power Appl. Syst.*, 1984, **PAS-103**, pp. 310–317
12 Chavez, J.J., Ramirez, A.: 'Dynamic harmonic domain modeling of transients in three-phase transmission lines', *IEEE Trans. Power Deliv.*, 2008, **23**, (4), pp. 2294–2301
13 Nguyen, H.V., Dommel, H.W., Marti, J.R.: 'Direct phase domain modelling of frequency dependent overhead transmission lines', *IEEE Trans. Power Deliv.*, 1997, **12**, (3), pp. 147–157
14 Gustavsen, B., Semlyen, A.: 'Combined phase domain and modal domain calculation of transmission line transients based on vector fitting', *IEEE Trans. Power Deliv.*, 1998, **13**, (2), pp. 596–604
15 Dommel, H.W., Yan, A., Wei, S.: 'Harmonics from transformer saturation', *IEEE Trans. Power Syst.*, 1986, **PWRD-1**, (2), pp. 209–215
16 Bollen, M.H.J., Gu, I.Y.H.: 'Signal processing of power quality disturbances' (IEEE Press, John Wiley & Sons, 2006)

8 Appendix 1: transmission line model in the DHD

Focusing on bus n, the relation between the incident current, i'_n, and the reflected current, i''_m, is

$$i'_n = H_{\text{mode}} i''_m \tag{28}$$

Approximating H_{mode} by rational functions, (31) is expressed as

$$i'_n = [c_1(s\boldsymbol{I} - \boldsymbol{A}_1)^{-1}\boldsymbol{b}_1]i''_m \tag{29}$$

The set of poles obtained from the rational fitting are contained in the diagonal matrix $\boldsymbol{A}_1$; the column vector $\boldsymbol{b}_1$ has all entries equal to '1' and the residues of the realisation are contained in the row vector $\boldsymbol{c}_1$. Thus the corresponding state–space realisation for (32) becomes

$$\boldsymbol{x}_1 = \boldsymbol{A}_1\boldsymbol{x}_1 + \boldsymbol{b}_1 i''_m \tag{30}$$

The state–space realisation for the two line nodes, m and n, in the DHD becomes (8), with the following matrix definitions with corresponding dimensions shown in parentheses (for k poles and h harmonics)

$$\boldsymbol{A}_1 = \text{diag}\{a_1\boldsymbol{I}_h, a_2\boldsymbol{I}_h, \ldots, a_k\boldsymbol{I}_h\}, \quad (kh \times kh)$$
$$\boldsymbol{S}' = \text{blkdiag}\{\boldsymbol{S}, \boldsymbol{S}, \ldots, \boldsymbol{S}\}, \quad (kh \times kh)$$
$$\boldsymbol{B}_1 = [\boldsymbol{I}_h, \boldsymbol{I}_h \ldots \boldsymbol{I}_h]^{\text{T}}, \quad (kh \times h)$$
$$\boldsymbol{C}_1 = [\boldsymbol{c}_1\boldsymbol{I}_h, \boldsymbol{c}_2\boldsymbol{I}_h, \ldots, \boldsymbol{c}_k\boldsymbol{I}_h], \quad (kh \times h)$$

$\boldsymbol{I}_h$ corresponds to the identity matrix of dimensions $(h \times h)$

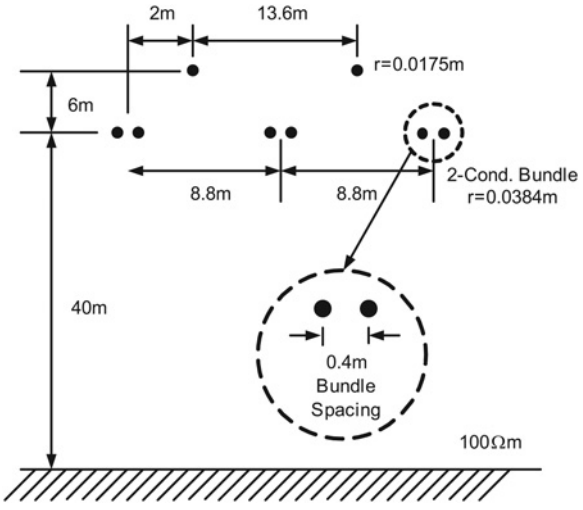

Fig. 11 *Untransposed transmission line configuration*

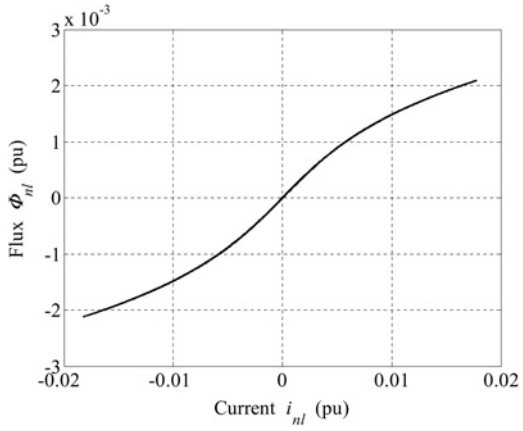

Fig. 12 *Non-linear load magnetic saturation characteristic*

and the time delay for all harmonics is taken into account by

$$\Gamma = \text{diag}\{e^{jh\omega_o\tau}, \ldots, e^{j\omega_o\tau}, 1, e^{-j\omega_o\tau}, \ldots, e^{-jh\omega_o\tau}\}$$

9 Appendix 2: line configuration

The geometrical configuration for the untransposed transmission line used in Section 4 is shown in Fig. 11.

10 Appendix 3: non-linear load magnetising characteristic

The magnetic saturation characteristic of the non-linear load ($\Phi - i$ curve) is presented in Fig. 12.

doi: 10.1049/iet-gtd.2010.0779